J|A|C|S COMMUNICATIONS

Published on Web 03/17/2009

Zeptomol Detection Through Controlled Ultrasensitive Surface-Enhanced Raman Scattering

Laura Rodríguez-Lorenzo,[†] Ramón A. Álvarez-Puebla,*[,†] Isabel Pastoriza-Santos,[†] Stefano Mazzucco,[‡] Odile Stéphan,[‡] Mathieu Kociak,[‡] Luis M. Liz-Marzán,[†] and F. Javier García de Abajo*[,§]

Departamento de Química-Física and Unidad Asociada CSIC-Universidade de Vigo, Vigo, Spain, Laboratoire de Physique des Solides, CNRS, UMR8502, Université Paris Sud XI, F91405 Orsay, France, and Instituto de Óptica, CSIC and Unidad Asociada CSIC-Universidade de Vigo, Serrano 121, 28006 Madrid, Spain

Received December 9, 2008; E-mail: ramon.alvarez@uvigo.es; jga@cfmac.csic.es

The ability of resolving the identity of molecular species in low concentration renders optical SERS analysis an excellent tool for ultrasensitive detection.[1,2] The low cross section of Raman molecular signals is typically overcome by means of large amplification especially at randomly encountered hot spots, particularly in nanostructured metals.[3] However, the detailed geometry and performance of such hot spots is well understood,[4−8] but their controlled fabrication is not, thus hindering the availability of controlled, quantitative SERS analysis. In this communication, we demonstrate controllable SERS signal amplification of $\sim 10^{10}$, exceeding what was previously thought possible only at randomly occurring particle aggregates.[9]

SERS largely relies on collective oscillations of conduction electrons in metals, which interact with light to produce high confinement of electromagnetic energy, particularly in narrow gaps between metal nanoparticles, but also at sharp nanoscaled corners and edges.[10,11] These so-called localized surface plasmons can encompass intensity enhancement factors of up to 5 orders of magnitude at visible and near-infrared (vis−NIR) frequencies in metals such as Ag and Au,[9] which directly translates into an increase of electronic transition probabilities of atoms or molecules exposed to such fields. In particular, surface-enhanced Raman scattering by molecules starts with an excitation, followed by inelastic coupling to internal vibrational levels of the molecule and a subsequent radiative decay, thus involving two electronic transitions, and therefore undergoing signal enhancement factors up to 10 orders of magnitude by coupling to plasmonic hot spots.[9]

Such a tremendous increase in SERS signal allows zeptomole detection.[12] However, SERS is typically performed on nanostructured metal surfaces, where plasmon hot spots are randomly distributed and little is known about the precise geometry and detailed mechanisms leading to such large field enhancements. This prevents accurate, quantitative SERS analysis. Recent attempts to produce quantitative, high-yield SERS have relied on optical field concentration at the gaps between aggregated particles,[9] but these systems are difficult to control, and their reproducibility is ruined by inescapable finite distributions of particle sizes and gap widths.[5] Other imaginative approaches using plasmon standing waves[13] and Wood anomalies in gratings[14] sacrifice the maximum achievable enhancement to gain controllability in return.

Herein we demonstrate a simple experiment that yields quantitatively controlled SERS enhancement factors beyond what has ever been thought possible. A sketch of the experimental system is shown in Figure 1a and involves the following steps: (i) A small fraction of the molecules to be sampled (1,5-naphtalenedithiol, 15NAT, in our proof-of-principle experiment) is randomly dispersed within a self-assembled monolayer of longer, dummy molecules with a low SERS cross section[15] (1-octanethiol, 1OT in what follows), which is deposited on an optically thick Au substrate; both 15NAT and 1OT molecules contain thiol groups through which they easily bind onto the Au substrate. (ii) Au nanostars[16] are then assembled on the molecule-decorated Au substrate. (iii) In contrast to 1OT, which contains a single thiol group through which it attaches to the planar Au surface, the probed molecules 15NAT contain a second thiol group that sticks out of the substrate and is thus available for the nanostars to bind on, preferentially through their tips, which are more easily penetrating through the bed of the longer 1OT

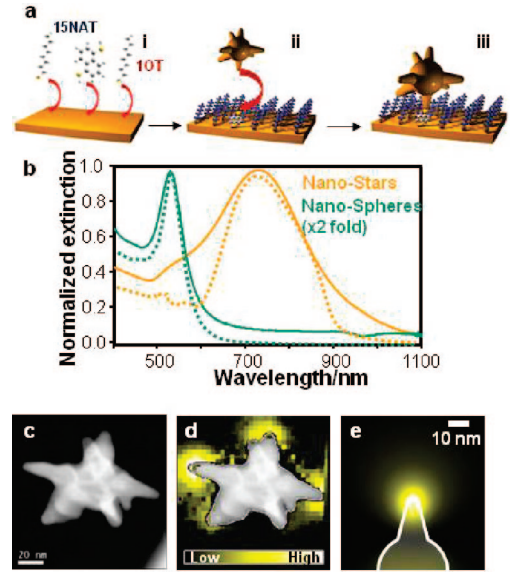

Figure 1. Preparation and characterization of single-particle plasmon resonances. (a) Controlled film fabrication for the deposition of single particles onto single molecules. A self-assembled monolayer comprising a large fraction of 1OT and a small fraction of 15NAT molecules is assembled on a smooth Au film (i), which is subsequently immersed in a Au nanostar colloid (ii). Nanoparticles are selectively retained by 15NAT, as 1OT is inert to them (iii). (b) Experimental (solid curves) and calculated (broken curves) extinction spectra in water for spherical (46 ± 4 nm) and star-shaped (41 ± 8 nm) Au colloids. All spectra are normalized to their maximum. (c) High resolution STEM dark-field image of a single Au nanostar. (d) EELS intensity mapping over the same particle. (e) Calculated EELS intensity map of the plasmon resonance in a particle tip, showing high localization near the tip apex, in agreement with the observed EELS image.

[†] Departamento de Química-Física and Unidad Asociada CSIC-Universidade de Vigo.
[‡] Université Paris Sud XI.
[§] Instituto de Óptica, CSIC and Unidad Asociada CSIC-Universidade de Vigo.

10.1021/ja809418t CCC: $40.75

molecules. Optical hot spots are then formed in the gaps between nanostar tips and the planar Au surface. The dimensions of these gaps are determined by the length of the probed molecules (~1 nm for 15NAT). The main goal of this procedure is to facilitate that each hot spot contains one or very few 15NAT molecules, since their density in the self-assembled monolayer is much lower than that of 1OT molecules.

The enhancement at the gap between nanostar tips and the Au substrate is facilitated by highly localized plasmons at the former. We show in Figure 1b a measured extinction spectrum for Au nanostars dispersed in water, as compared to that for Au nanospheres. Details on the synthesis and characterization methods of both types of particles are given in the Supporting Information (SI). The stars display two plasmon modes, one of them being localized at the tips and producing a dominant broad feature at the edge of the visible range (~730 nm).[16] This mode overlaps the laser wavelength employed in our SERS measurements (785 nm), which was chosen to avoid photodegradation of the probed molecules. In contrast, Au nanospheres produce a narrower band at shorter wavelengths (~530 nm). Experimental evidence for the spatial distribution of these plasmon modes is provided by electron energy-loss spectroscopy (EELS) mapping (Figure 1d) performed on a single particle in a scanning transmission electron microscope (STEM), similar to recent benchmark studies of plasmon mapping on silver nanoprisms.[17] This mapping clearly demonstrates the highly localized character of the lowest energy plasmons at the tips. Boundary element method (BEM) calculations[18,19] are in excellent agreement with both the spectral features of the extinction spectra (dashed curves, Figure 1b) and the EELS-resolved tip-plasmon spatial distribution (Figure 1e) (see SI for further details). The red shift of the tip mode with respect to the plasmon localized at the central sphere is consistent with the intuition gathered from a similar effect occurring in longitudinal excitations of elongated particles as either the aspect ratio or the tip sharpness are increased[20] (see Figure S3 in the SI).

The degree of SERS amplification measured in our experimental system is illustrated in Figure 2a, in which the SERS spectrum (red line) is compared to a Raman spectrum acquired for 15NAT molecules in the liquid phase (blue line). Both spectra are normalized to count rate per 15NAT molecule. An overall ~10^{10} SERS enhancement factor is determined from these measurements. Signal normalization required detailed molecule (nanostar) counting, as described in the SI. It should be noted that the S−H stretching vibrational mode (2562 cm^{-1} in the bulk Raman spectrum, see Table S1 in the SI) is not present in the SERS spectrum, which confirms the covalent binding of the thiol group to Au.[21] The SERS signal from individual hot spots (i.e., individual 15NAT molecules) can be clearly resolved in a sample with a sparse distribution of 15NAT molecules (see Figure 2c, with a 15NAT:1OT molar ratio of 1:1000), using Raman features that are easily discerned in the spectra. A more concentrated sample (Figure 2b, corresponding to a 15NAT:1OT ratio of 1:100) reveals the same features, with a better signal-to-noise ratio, which we used for the quantitative assessment of the SERS enhancement factor.

Additional proof of the importance of using particles with sharp tips was obtained by repeating these measurements using nanospheres rather than nanostars. Nanospheres lead to SERS enhancement factors that are roughly over 2 orders of magnitude smaller than those from nanostars (Figure 3). The array of nanospheres considered in Figure 3a, which has a larger particle density than the array of nanostars shown in Figure 2b, still results in a low count rate and a relatively noisy SERS signal, unlike the spectrum obtained with nanostars. Additionally, Figure 3b shows that, in

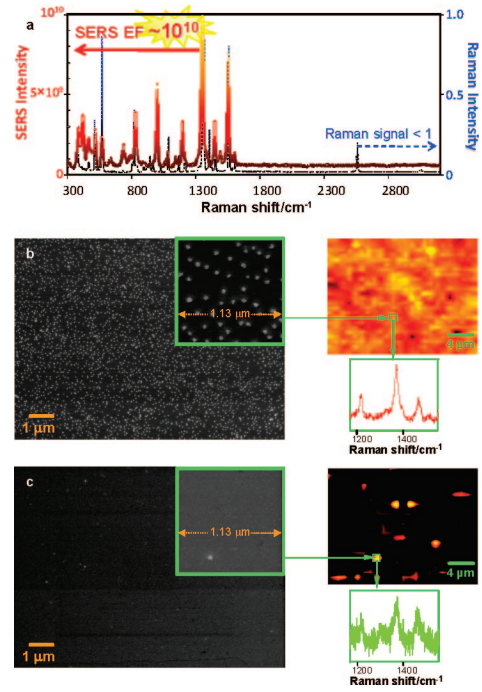

Figure 2. Raman and SERS spectra at hot spots. (a) Bulk Raman spectrum of 15NAT molecules in aqueous solution (right scale), compared to the SERS spectrum of the same molecules recorded by using the scheme of Figure 1a with nanostars (left scale). The 1OT:15NAT ratio is 100:1. The nanostar-assisted SERS signal per molecule is ~10^{10} times larger than the Raman signal per molecule (enhancement factor EF ~10^{10}). (b) Left: SEM images showing bound nanoparticles with a density of 27 ± 7 particles per μm^2. Right: SERS spatial mapping over the highlighted region in the SEM image. (c) Single-particle SERS mapping recorded from a sample with less than 1 particle per μm^2. Details of SERS spectra collected within an area of 1.28 μm^2 are shown for the samples in images b and c.

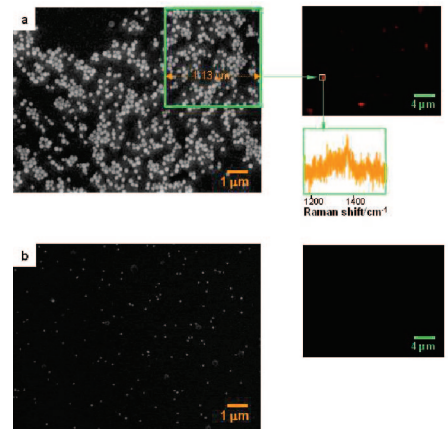

Figure 3. (a) Left: SEM images showing bound spherical nanoparticles with a density of 198 ± 28 particles per μm^2. Right: SERS spatial mapping over the highlighted region in the SEM image. (b) Left: SEM image of bound spheres at density lower than 1 particle per μm^2 (single molecule regime). Right: SERS mapping showing no evidence of vibrational peaks of the probed molecule.

contrast to nanostars, zeptomole detection with nanospheres is unattainable and results in a SERS count rate below the noise level, thus producing a blank SERS map (cf. Figures 3b and 2c).

Our main results are summarized in Figure 4, and in particular Figure 4d presents a comparison of theory and experiments for SERS with nanospheres and nanostars at three different Raman lines (see assignment of the 15NAT Raman lines in Table S1, SI). The upper panel contains sketches and BEM calculations of the SERS

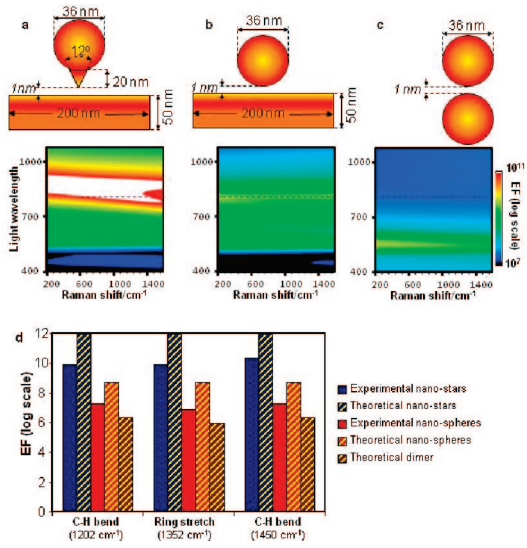

Figure 4. SERS enhancement factor. (a−c) Schematic representation and calculated SERS enhancement factor as a function of Raman shift and laser wavelength for three different nanostructured Au configurations: (a) a sphere with a tip near a plate (tip semiangle equal to 12°, as deduced from TEM images; see Figure S3 in SI for influence of tip geometry), (b) a sphere near a plate, and (c) a Au sphere dimer. (d) Measured and calculated enhancement factors for all these systems at selected Raman peaks (see Table S1 in the SI).

enhancement for three different nanostructured Au configurations: tip−surface and sphere−surface configurations mimicking the measured nanostar- and nanosphere-assisted SERS, and a nanosphere dimer as considered in earlier studies.[9] The calculated enhancement factor is plotted as a function of incident light wavelength and Raman shift for a surface-to-surface gap of 1 nm in all cases, consistent with the size of the 15NAT molecule used in the present experiments. The enhancement is clearly higher for the nanostars, both for the excitation wavelength under consideration and as compared to the maximum enhancement predicted for the other two configurations. This behavior is fully consistent with our measurements, and the results for the sphere dimer are also in agreement with previous calculations.[4,9] The relevant role of the flat Au surface in SERS amplification is clearly illustrated by these calculations. We compare in Figure 4d experimental and calculated SERS enhancement factors for nanostars and nanospheres. As expected, the sphere with a tip gives rise to a considerably larger overall enhancement than the sphere with no tip. Calculated values are a little higher than the corresponding experimental ones (10^{12} vs 10^{10} for the sphere with a tip and 10^9 vs 2.3×10^8 for the regular sphere). There are several reasons to which this difference could be ascribed: worse coincidence of the laser wavelength with hot-spot resonances; poor performance of some of the tips (e.g., the smoother ones); or nonlocal effects, which effectively smooth the metal boundaries with respect to the sharp interface description inherent in customary local calculations of the light field for metal-to-metal gap distances below 1−2 nm.[22] However, the calculated difference in the enhancement factors between the tip and the sphere configurations (2−3 orders of magnitude) is in close agreement with the experimentally measured 250-fold increase.

The procedure herein reported thus provides a simple way of achieving reproducible, ultrasensitive SERS spectroscopy for zeptomole detection. The method can be easily applied to other types of molecules. For fixed dimensions of the exciting laser spot, the ratio of probed to dummy molecules (see Figure 1a) determines the sensitivity of the technique (i.e., the intensity of the spectra and the number of emitting molecules) and solves the problem of quantitative detection with high-throughput. Our controllable hot spots open a new avenue toward nonlinear optics (e.g., for all-optical switching and up-conversion applications). They should also be useful as nanoantennas for coupling laser light into plasmon polaritons, while textured Au surfaces could be a practical solution for high-throughput screening, biosensing and diagnosis, combinatorial chemistry, and drug discovery.

Acknowledgment. We thank B. Rodríguez-González for assistance with SEM measurements. Supported by the Spanish MEC (Consolider Nanolight.es, MAT2007-62696, and MAT2007-66050), Xunta de Galicia, and the EU (NMP4-2006-016881-SPANS, NMP4-SL-2008-213669-ENSEMBLE, FP7-213948-2-NANODIRECT, I3-026019-ESTEEM, and Marie Curie MEST CT 2004 514307).

Supporting Information Available: Experimental Section, TEM images, and BEM calculations. This material is available free of charge via the Internet at http://pubs.acs.org.

References

(1) Aroca, R. F. *Surface Enhanced Vibrational Spectroscopy*; Wiley: New York, 2006.
(2) De Angelis, F.; Patrini, M.; Das, G.; Maksymov, I.; Galli, M.; Businaro, L.; Andreani, L. C.; Di Fabrizio, E. *Nano Lett.* **2008**, *8*, 2321–2327.
(3) Lee, S. J.; Guan, Z.; Xu, H.; Moskovits, M. *J. Phys. Chem. C* **2007**, *111*, 17985–17988.
(4) Bidault, S.; García de Abajo, F. J.; Polman, A. *J. Am. Chem. Soc.* **2008**, *130*, 2750–2751.
(5) Braun, G.; Pavel, I.; Morrill, A. R.; Seferos, D. S.; Bazan, G. C.; Reich, N. O.; Moskovits, M. *J. Am. Chem. Soc.* **2007**, *129*, 7760–7761.
(6) Camden, J. P.; Dieringer, J. A.; Wang, Y.; Masiello, D. J.; Marks, L. D.; Schatz, G. C.; Van Duyne, R. P. *J. Am. Chem. Soc.* **2008**, *130*, 12616–12617.
(7) Laurence, T. A.; Braun, G.; Talley, C.; Schwartzberg, A.; Moskovits, M.; Reich, N.; Huser, T. *J. Am. Chem. Soc.* **2009**, *131*, 162–169.
(8) Kneipp, J.; Li, X.; Sherwood, M.; Panne, U.; Kneipp, H.; Stockman, M. I.; Kneipp, K. *Anal. Chem.* **2008**, *80*, 4247–4251.
(9) Xu, H.; Bjerneld, E. J.; Käll, M.; Borjesson, L. *Phys. Rev. Lett.* **1999**, *83*, 4357–4360.
(10) Hao, E.; Bailey, R.; Schatz, G.; Hupp, J. T.; Li, S. *Nano Lett.* **2004**, *4*, 327.
(11) Prodan, E.; Radloff, C.; Halas, N. J.; Nordlander, P. *Science* **2003**, *302*, 419.
(12) Pieczonka, N. P. W.; Aroca, R. F. *Chem. Soc. Rev.* **2008**, *37*, 946–954.
(13) Abdelsalam, M.; Bartlett, P. N.; Russell, A. E.; Baumberg, J. J.; Calvo, E. J.; Tognalli, N. s. G.; Fainstein, A. *Langmuir* **2008**, *24*, 7018–7023.
(14) Brolo, A. G.; Arctander, E.; Gordon, R.; Leathem, B.; Kavanagh, K. L. *Nano Lett.* **2004**, *4*, 2015–2018.
(15) Constantino, C. J. L.; Lemma, T.; Antunes, P. A.; Aroca, R. *Anal. Chem.* **2001**, *73*, 3674–3678.
(16) Kumar, P. S.; Pastoriza-Santos, I.; Rodríguez-González, B.; García de Abajo, F. J.; Liz-Marzán, L. M. *Nanotechnology* **2008**, *19*, 015606.
(17) Nelayah, J.; Kociak, M.; Stéphan, O.; García de Abajo, F. J.; Tencé, M.; Henrard, L.; Taverna, D.; Pastoriza-Santos, I.; Liz-Marzán, L. M.; Colliex, C. *Nat. Phys.* **2007**, *3*, 348–353.
(18) García de Abajo, F. J.; Howie, A. *Phys. Rev. Lett.* **1998**, *80*, 5180–5183.
(19) García de Abajo, F. J.; Howie, A. *Phys. Rev. B* **2002**, *65*, 115418.
(20) Myroshnychenko, V.; Rodríguez-Fernández, J.; Pastoriza-Santos, I.; Funston, A. M.; Novo, C.; Mulvaney, P.; Liz-Marzán, L. M.; García de Abajo, F. J. *Chem. Soc. Rev.* **2008**, *37*, 1792–1805.
(21) Alvarez-Puebla, R. A.; Dos Santos, D. S., Jr.; Aroca, R. F. *Analyst* **2004**, *129*, 1251–1256.
(22) Garcia de Abajo, F. J. *J. Phys. Chem. C* **2008**, *112*, 17983–17987.

JA809418T